JOURNAL OF MATERIALS SCIENCE:MATERIALS IN MEDICINE 7 (1996) 207–213

A quantitative technique for comparing synthetic porous hydroxyapatite structures and cancellous bone

K. O'KELLY, D. TANCRED, B. McCORMACK, A. CARR
Department of Mechanical Engineering, University College Dublin, Ireland

There are many different materials currently available for cancellous bone grafting. There is however, very little information relating the morphology of these materials to cancellous bone. Work was undertaken to develop a quantitative method for comparing synthetic hydroxyapatite bone structures with cancellous bone. The bases for comparison were mean plate thickness, mean plate distance, mineral area fraction, mineral volume fraction and plate orientation coupled with mechanical tests. The aim of this work was to develop a protocol for assessing whether these critical parameters which influence the success of bone implants were achieved in the synthetic materials. The methodology is successful in providing quantitative information about the mineral area fraction, the mean plate distance or pore size and the intercept frequency as a function of angle. Combining these three provides a quantitative measure of how much mineral there is and how it is distributed and oriented. The mechanical tests yield strengths and moduli values based on apparent density. The results of the mechanical tests can also be plotted as functions of the more discrete structural features such as those quantified in the image analysis to allow for even more equitable and systematic comparisons of different porous materials.

1. Introduction

It has long been accepted that cancellous bone microstructure has a profound influence on the rate of ingrowth into bone grafts. Similarly, material composition also plays a significant role in the process [1–7]. Thus most research into bone grafting has focused on duplicating the structure and material of cancellous bone using natural and synthetic structures. For all such materials, it is necessary to quantify the structural, material and mechanical properties so that comparisons can be made to natural bone for selection purposes.

DeHoff [8] classified the geometric properties of three-dimensional structures into: Class I – standard stereological properties, estimated without geometric assumptions, Class II – properties that require geometric assumptions for their estimation and Class III – properties that cannot be estimated stereologically. Although Class I measurements are the most straightforward, they provide information that is too specific for the purposes of classifying cancellous bone and grafting materials by key structural features. The Class I measurements would yield an enormous number of types when applied to the range of architectures. These would have to be rationalized and generalized to yield a manageable group of structural families. Class II properties do compromise the specificity of Class I measurements by requiring some geometric assumptions to be made but are far more useful when trying to classify an almost infinite number of bone structures. Class III properties are almost impossible to quantify and so are used almost exclusively for qualitative descriptions.

There has been a great deal of work done in trying to identify key structural features that sufficiently differentiate the types of cancellous bone. The approaches have used all three types of geometric properties and have included porous block models [9], node–strut models [10, 11] and star volume models [12]. Singh [13] classified cancellous bone into seven types based on shapes, thicknesses and orientations of the rods and plates. The qualitative nature of these classifications is useful in making general comparisons between cancellous bone in different loci but makes it difficult to compare structures of different materials. Other methods include using three-dimensional connectivity (Euler number/tissue volume) [14]; the trabecular bone channel density (no. of channels/cm^2 of tissue area) [5]; the ratio of nodes to free ends and lengths of different strut types expressed as a percentage of total strut lengths [15]; a probability distribution function of porosity and an autocorrelation function describing the probability of a point being part of the matrix [16].

Most work, however, has centred on the Class II type properties of bone: mean trabecular plate thickness, mean trabecular plate distance or mean pore size, bone area fraction, bone volume fraction and principal axes or orientation. The distinguishing aspect of research in this area has been the methods used to measure and derive these quantities [7, 17–19].

0957–4530

There has also been a great deal of work using various forms of image analysis to directly measure specific and mean properties [20–27].

This research group has been involved with the production of various synthetic porous hydroxyapatite structures which reproduce, as much as possible, the key physical and material features of cancellous bone. In doing so, much effort has gone into developing a method for measuring these features to allow quantitative comparisons between synthetic structures and cancellous bone. This paper presents a protocol for characterizing cancellous bone and the various grafting materials, both natural and synthetic. This protocol incorporates structural comparisons using image analysis, mechanical comparisons using compression and shear tests and direct mineral volume calculations. As an example the protocol is applied to bovine cancellous bone and two synthetic hydroxyapatite structures developed by the research group.

2. Materials

The experimental data were taken from three different materials: natural bovine bone and two synthetic porous hydroxyapatite–glass structure of different mixtures: 75%–25% and 50%–50%. Because the image analysis is a non-destructive procedure, we were able to reduce the sample numbers by carrying out image analysis prior to mechanical testing. In order to make comparisons of material properties we removed all organic matter from the bone specimens.

2.1. Bone

Bone samples were taken from the distal lateral femoral condyle of 10 fresh bovine femurs aged less than 3 years. Large slices ($w = 8$ mm) were obtained and initially cleaned with a degreasing agent for 2–5 min prior to soaking in ethylene diamine for 48 h to remove all organic matter. These large slices were then cut down to cubes of $l = 12$ mm (anterior–posterior), $w = 8$ mm (lateral–medial), $h = 10$ mm (proximal–distal) of which 42 were selected for testing. Selection was based on apparent density measurements and visual checks for structural homogeneity. Random samples were broken and viewed under scanning electron microscope (SEM) to confirm the removal of collagen fibres from the matrix.

2.2. 50/50 and 75/25 synthetic structures

The synthetic structures were composed of stoichiometric hydroxyapatite (HA) [$Ca_{10}(PO_4)_6(OH)_2$] and biological glass [SiO_2–Na_2O–CaO–Al_2O_3–B_2O_3], in different ratios. Both were synthesized in-house using standard protocols [28, 29]. X-ray diffraction tests on the HA confirmed the composition and also revealed approximately 8–10% tricalcium phosphate (TCP). Mean particle size was < 1 μm. Biological glass was chosen because of its non-toxic effect. Glasses with alumina and borosilicate were tried and yielded better results but were discounted because of the negative biological effect.

The subsequent processes were manipulated to try and yield specific structural characteristics and mechanical properties similar to those of real bone. The process is still under development but is sufficient for this work in that it produced specimens with bone-like features. The synthetic porous HA specimen sizes were nominally 12 mm × 10 mm × 8 mm. Radiographic images were used to eliminate structurally inhomogeneous specimens.

3. Comparison methods

Samples from the three material groups were subjected to image analysis for structural comparisons, and compression and shear tests for comparison of material properties.

3.1. Image analysis (structural properties)

Image analysis was carried out on the proximal and distal faces of the samples prior to mechanical testing. The images were obtained using a video framegrabber (Creative Labs Video Blasxter SE™) linked directly to image enhancing software where the images were converted to binary format and exported to the NIH Image 1.54 software. The video image and resulting binary image for bovine cancellous bone and a sample of synthetic porous HA are shown in Fig. 1a–d. The scale of the images was approximately 35 pixels/mm. Customized macros were written to measure mean plate distance (MPD), the mineral area fraction (MAF) and the principal axis of structural orientation. The mean plate thickness (MPT) could only be measured semi-automatically and proved too time-consuming to include in this study. MPD was obtained by counting the number of pairs of mineral/void interfaces along a given line and dividing by the total void distance along that line. This was carried out for a number of lines in the horizontal and vertical directions to negate the influence of orientation. The number of orthogonal lines is a user-defined option. MAF was calculated as the ratio of mineral pixels in the binary image to the total number of pixels. The measurement of orientation was made by calculating the number of mineral/void interfaces as a function of angle and plotting the results on a polar grid. The user is prompted for the angular increment, specimen details, and the orientations of the top and left side of the image to reference the localized orientation of trabeculae to global bone orientation.

3.2. Mechanical testing (material properties)

Both compression and shear tests were carried out on a Lloyd 6000S Materials Testing Machine using a 500 N load cell, in air at room temperature. For the bone specimens, the load direction was along the axis of natural loading (proximal–distal). The synthetic structures were loaded along the same geometric axis to preserve similarity. An auto-alignment rig was used for the compression tests. All compression tests were carried out at a constant displacement rate of 0.5 mm/min.

Shear tests were carried out in a special rig designed to constrain the material from bending and were

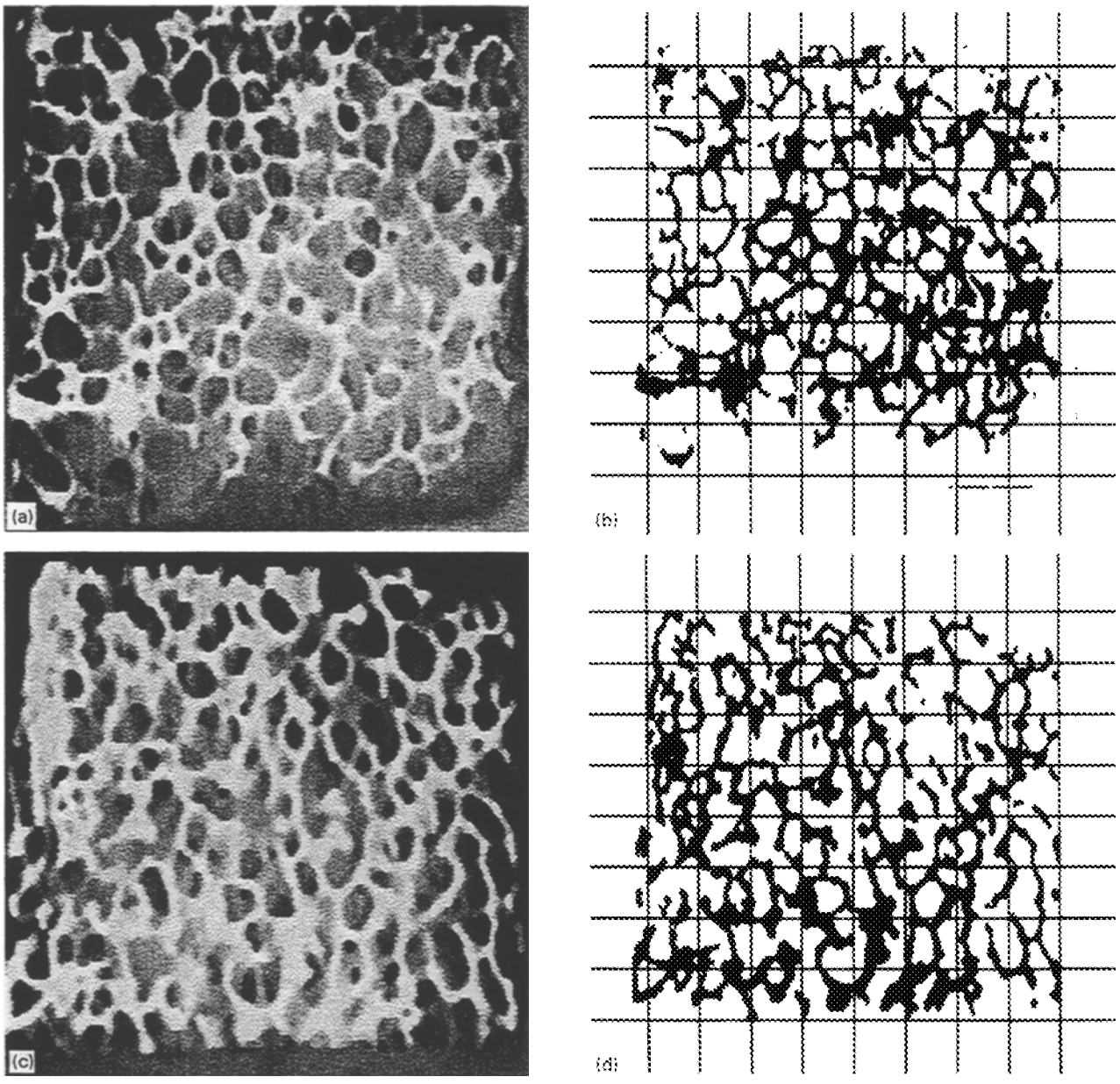

Figure 1 Video image of cleaned bovine cancellous bone (a) and the resulting binary image (b) generated using NIH Image. (c, d) The 50/50 synthetic structure. The grid represents the lines used to calculate MPD.

carried out at a constant displacement rate of 0.5 mm/min. Other rates were not used in either compression or shear since all three materials were mineral phase only and it is assumed that viscoelastic behaviour arises from the organic constituents of bone [30, 31].

The compressive and shear strengths, Young's and shear moduli are all reported as apparent material properties due to their dependence on the apparent density. Comparisons were also made between the mineral volume fractions (MVF) of bone and the two synthetic HA structures using Eq. 1.

$$\text{Ratio of MVFs} = \frac{\left(\frac{V_{HA}}{V_{HA\ Specimen}}\right)}{\left(\frac{V_{Bone}}{V_{Bone\ Specimen}}\right)} = \left(\frac{V_{Bone\ Specimen}}{V_{HA\ Specimen}}\right)\left(\frac{m_{HA}}{m_{Bone}}\right)\left(\frac{\rho_{Bone}}{\rho_{HA}}\right) \quad (1)$$

4. Results

4.1. Mechanical tests

The results of the compression and shear tests are shown in Figs 2–5. The mechanical material properties are all plotted on the vertical axes against apparent density (kg/m^3) on the horizontal axes. Figs 2 and 4 include data for bone and both synthetic HA structures whereas Figs 3 and 5 only show data for bone and the 50/50 synthetic structures. The omission of 75/25 data is due to insufficient specimen numbers arising from the radiographic images which revealed flaws in the batch of shear test specimens.

Figure 2 shows the behaviour of compressive strength for all three materials as a function of apparent density. Both synthetic materials are substantially weaker than bone. Within the range observed, 50/50 HA would require almost 40% greater apparent density to achieve the same strengths as bone while the 75/25 would require almost 70% greater apparent density. The shear test results (Fig. 3) show a similar

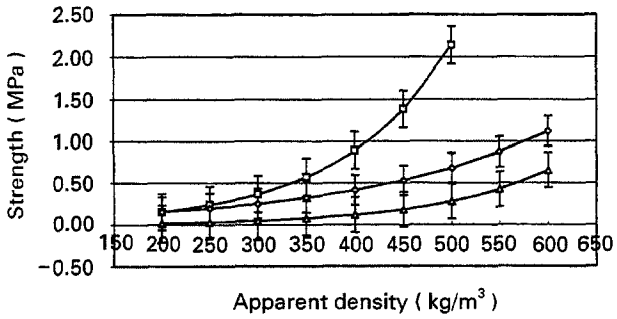

Figure 2 Compressive strength plotted against apparent density for cleaned bone (-□-), 50/50 (-◇-) and 75/25 (-△-) synthetic porous HA structures.

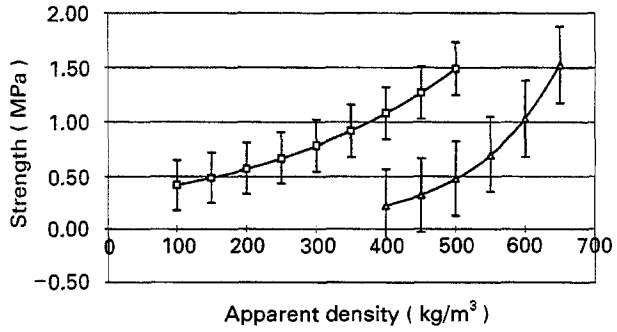

Figure 3 Shear strength plotted against apparent density for cleaned bone (–□–) and 50/50 (–△–) synthetic porous HA structures.

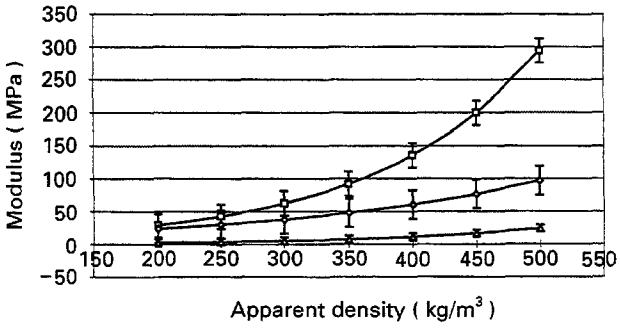

Figure 4 Young's modulus (E) plotted against apparent density for cleaned bone (–□–), 50/50 (–◇–) and 75/25 (–△–) synthetic porous HA structures.

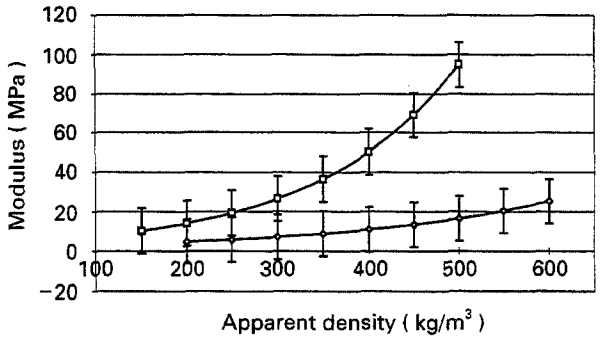

Figure 5 Shear modulus (G) plotted against apparent density for cleaned bone (–□–) and 50/50 (–◇–) synthetic porous HA structures.

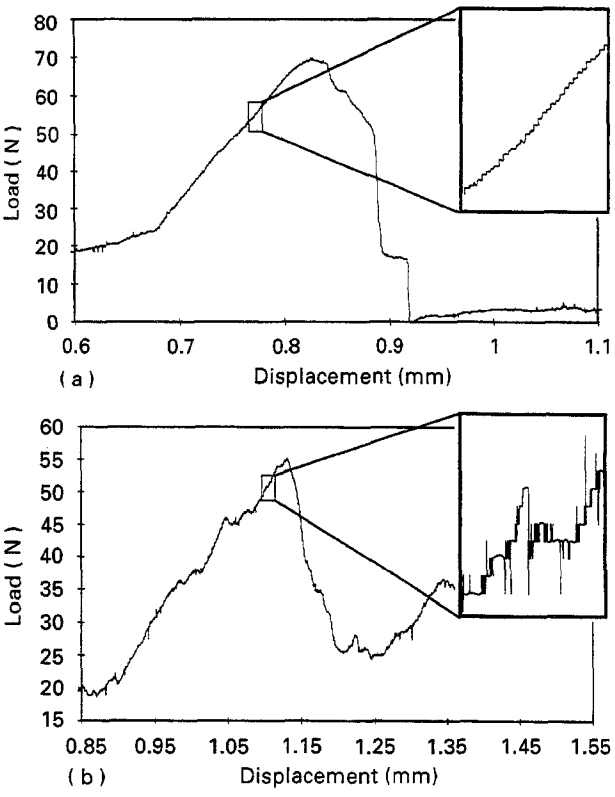

Figure 6 Representative load–displacement plot of compression test and the exploded view revealing the relative smoothness of the curve used to calculate E for (a) bone and (b) 50/50. The exploded view shows the jogging that occurs in the synthetic material at a microstructural level. This permanent deformation appears to contribute strongly to the lower moduli of the synthetic porous HA structures.

pattern. 50/50 requires about a 30% increase in apparent density to achieve the same strengths as bone.

Both the elastic and shear moduli results (Figs 4 and 5) follow the trends expected from the literature. Detailed examination of the load–displacement data (Fig. 6a, b) and SEM images of the structures reveal that the low moduli for both synthetic HA structures arise from collapsing of the microstructure due to a high level of microporosity. Thus it must be questioned whether the synthetic specimens exhibited pure elastic behaviour up to macroscopic failure. It should be noted that the values on the vertical axes are not intended to indicate absolute values of the material properties. The influence of specimen shape [32, 33] was not considered because we were only interested in comparisons between the three materials. Because of this, the equations describing the regression curves cannot be used for independent determination of material properties.

The mineral volume fraction was determined using Eqn. 1 and the results are shown in Table I. In both the 50/50 and 75/25 groups, the mean achieved MVF was only 84% that of bone. The difference between the 50/50 and 75/25 groups was 3.5% compared to 5% between the groups of bone that each was being processed to mimic.

4.2. Image analyses

Image analysis results were gathered for each specimen. The data includes the mean plate distance (MPD), the mineral area fraction (MAF) and principal orientation. This data was collected for the proximal and distal faces of 77 specimens. No distinction was made between 50/50 and 75/25 for the image analyses

TABLE I Mean values of mineral volume fraction for bone, 50/50 HA and 75/25 HA

Mean MVF		Mean MVF	
Bone	20.5% ± 3.3%	Bone	16.3% ± 2.3%
50/50	17.2% ± 2.3%	75/25	13.8% ± 1.3%
Mean difference	3.3% ± 2.7%	Mean difference	2.4% ± 2.7%
Ratio of mean MVFs	83.9%	Ratio of mean MVFs	84.7%

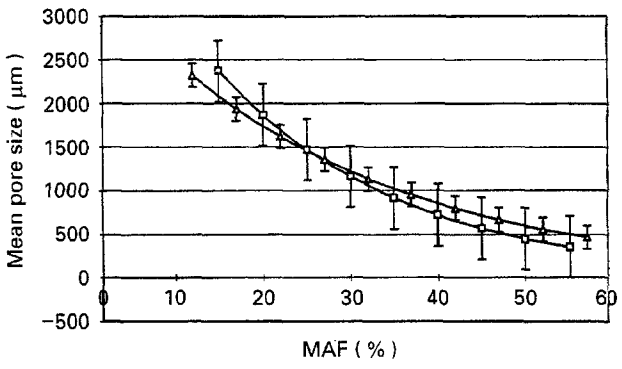

Figure 7 MPD plotted against MAF showing the distribution of material for a given MAF and the close agreement between bone (–□–) and synthetic HA structures (–△–).

since the processes to generate physical features was identical. Fig. 7 shows the MPD plotted against the MAF for bone and synthetic porous HA. By representing the data in this way, conclusions can be drawn about the distribution of mineral for a given MAF. For decreasing MAF we see an increase in MPD or mean pore size. Therefore, we can conclude that the materials have similar MAF and that the material itself is distributed over the area in a similar way. The standard error of estimate (SEE) is 136 μm for bone and 354 μm for 50/50. The correlation of each curve with the original data is good: $r = 0.87$ for bone and $r = 0.85$ for synthetic materials. More importantly, there is excellent agreement between the curves for bone and synthetic porous HA structures.

Representative results of principal plate orientation for bone and 50/50 are shown in Fig. 8a, b. Each specimen has a unique orientation so data reduction was not carried out. Fig. 9a, b merely indicate the degree to which orientation can be artificially created in the synthetic HA and how it compares to bone. The results have been plotted in polar co-ordinates to reveal the angles at which minimum and maximum intercept frequency occur.

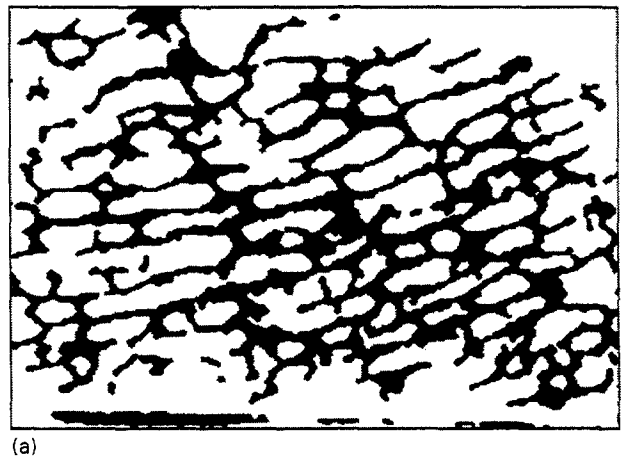

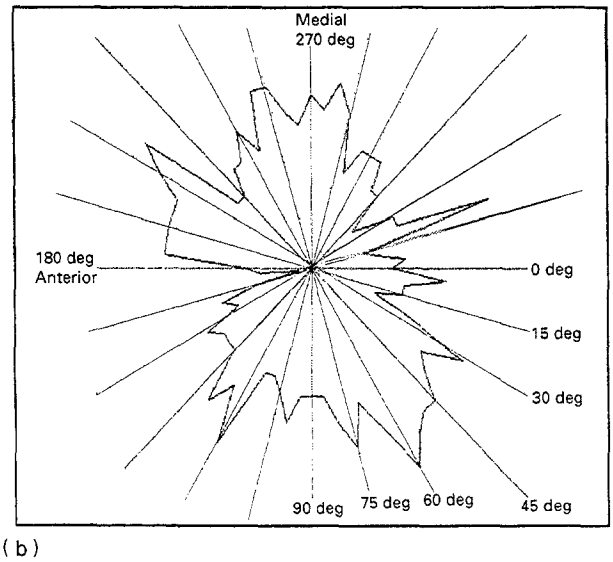

Figure 8 (a) Binary image of a strongly oriented cancellous bone and (b) the resulting polar plot generated by the image analysis. The plot shows a minimum intercept frequency along the axis of orientation.

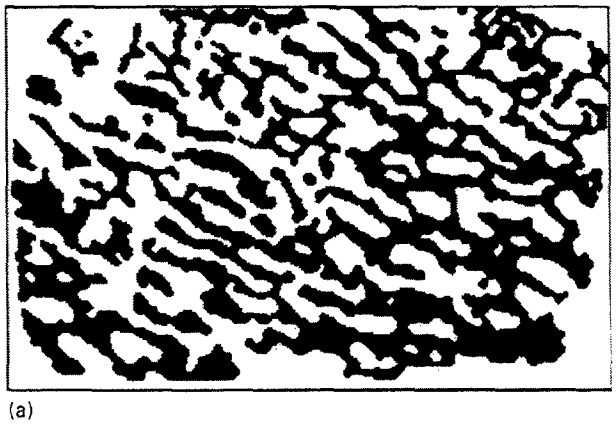

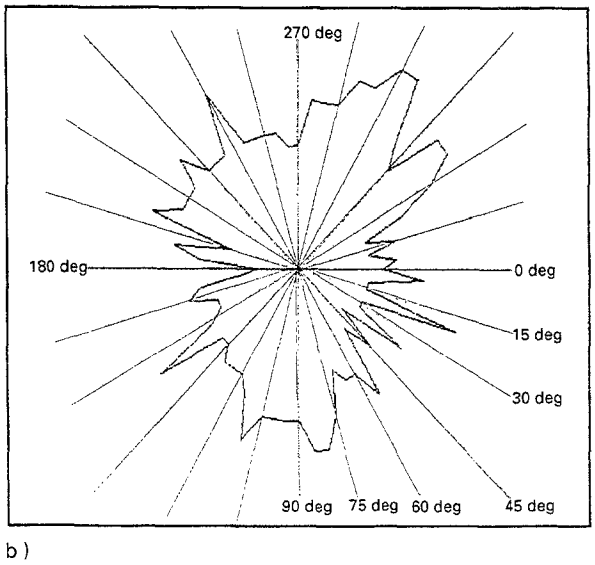

Figure 9 (a) Binary image of a 50/50 HA specimen processed to yield a strong orientation. The resulting polar plot (b) shows the similarity with bone in the angular distribution of intercept frequencies.

5. Discussion

There are a number of limitations with this work. The protocol does not make biological comparisons (e.g. resorption, remodelling characteristics). Nor does the work incorporate any comparison of the dynamic mechanical behaviour of the materials. The image analysis requires fairly large images in order to have high intercept counts. Preliminary trials with smaller samples (image area: 5 mm × 5 mm) yielded high standard deviations in the MPD measurements and inconclusive results in the orientation analyses. The specimen shape required for the image analysis is not ideal for the mechanical tests. In spite of the auto-alignment rig used in the compression tests, non-parallel planes did influence the crushing behaviour. Ideally, the shape should correspond to an accepted standard such as that defined by Keaveney *et al.* [33]. The mechanical properties presented in this paper can only be used for comparative purposes. Acknowledging these limitations, the results confirm that the protocol described here is an effective tool for making quantitative comparisons of key structural and mechanical features. It is, however, only the first study in developing a comprehensive comparative protocol.

5.1. Mechanical comparisons

The results clearly indicate that the synthetic HA structures are weaker than bovine bone in both compression and shear. The resulting elastic and shear moduli (Figs 4 and 5) show that the synthetic HA structures are far less stiff than the bone. Care was taken to factor out the contribution of collapsing pores (Fig. 6b) which show themselves in the data as sudden macroscopic jogs in the elastic region. However, closer examination indicates that lower moduli are due to permanent deformation occurring at the microstructural level due to high levels of microporosity in the synthetic HA specimens. This was supported by evidence during the compression tests that bone is reversible in loading in the elastic region whereas the synthetic HA structures showed small amounts of permanent deformation. This difference in microstructural behaviour is significant for those involved in processing synthetic bone grafting material. However, the results of the mechanical tests as well as qualitative observations of the synthetic specimens do indicate that the strengths of the specified shape are adequate for surgical procedures. Although too brittle to allow for substantial post-process shaping, the synthetic HA structures can tolerate fine shaping.

The MVF results show that control of the MVF was achieved by the two synthetic HA groups. Each achieved 84% of the targeted MVF. This shortfall is not significant from a biological point of view since the values for 50/50 and 75/25 fall within the 95% confidence interval of natural bone. However, the difference in mean values may partly explain the differences in compressive and shear strengths between the synthetic HA structures and bone. A MVF difference of 3.5% between 50/50 and 75/25 was achieved compared to the difference of 5% between the two groups of bone that were being mimicked.

5.2. Structural comparisons

The image analysis software proved successful for characterizing the defined structural features in both bone and the synthetic HA structures. The measure of orientation proved to be highly sensitive to the scale of the image. Small images yield low intercept frequencies which can be obscured by statistical fluctuations in the measurements. Thus, large images (larger than 10 mm × 10 mm) are required to provide high intercept counts and thereby improve the "signal to noise" ratio.

The image analysis showed that mean spacing between interconnectors was successfully duplicated in both the synthetic structures. Likewise it showed that the processing can manipulate the mineral area fraction corresponding to a range of typical cancellous bone densities. More significantly, the measurements of MPD and MAF show that the distribution of mineral in the synthetic HA structures was the same as that of bone with the same mineral area fraction. Finally, the analysis showed that a strong orientation can be created that closely matches that in cancellous bone.

6. Conclusions

The methodology provides a quantitative comparison between synthetic porous HA structures and cancellous bone. The mechanical tests show that the strengths in compression and shear require 40–50% greater apparent density to achieve the same performance as bovine cancellous bone. This may in part be due to a 16% lower mineral volume fraction in the synthetic HA structures. The image analysis, however showed that mean plate distance, or pore size, and mineral area fraction agree very well with those of bone. The orientation analysis also reveals that intercept frequencies in specific orientations can be created which closely match those of bone. The image analysis can be carried out at low cost; the only hardware required is a video camera and an Apple PC with framegrabber to run NIH Image©. A simpler though more cumbersome approach is to scan in photographic images, eliminating the need for video camera and framegrabber.

Thus, the protocol described in this paper provides a good cost-effective method for quantitatively comparing key structural and mechanical features. The features quantified by the image analysis provide a sensible basis for comparisons in terms of the mineral area fraction, the mean plate distance or pore size and the intercept frequency as a function of angle. Combining these three provides a quantitative measure of how much mineral there is and how it is distributed and oriented. Although the results are not presented in this paper, the protocol can describe yield strengths and moduli based on either apparent density, mean pore size, mineral area fraction or mean

plate thickness. This combination of mechanical and structural properties provides the basis for a more equitable and systematic method of comparing bone and bone-like structures.

Acknowledgements

The authors acknowledge the assistance of the Electron Microscopy Laboratory, UCD, Ireland and the IDA Newman Scholarship Fund.

References

1. L. C. ABBOTT, E. R. SCHOTTSTAEDT, J. B. SAUNDERS and F. C. BOST, *J. Bone Jt Surg.* **39** (1947) 381.
2. R. S. SIFFERT, *ibid.* **99** (1967) 746–755.
3. W. A. SOUTER, *ibid.* **51B** (1969) 63–75.
4. A. L. BOSKEY and A. S. POSNER, In Symposium on Metabolic Bone Disease, Orthopaedic Clinics of North America **15** (1984) 597–612.
5. K. SATO, E. WAKAMATSU, T. SATO, T. HONMA, H. KOTAKE and P. D. BYERS, *Calcified Tiss. Int.* **39** (1986) 2–7.
6. J. A. BUCKWALTER and R. R. COOPER, "Physiology of bone", American Academy of Orthopaedic Surgeons **26** (1987) 27–48.
7. L. D. HORDON and M. PEACOCK, *Bone and Mineral* **11** (1990) 335–345.
8. R. T. DeHOFF, *J. Microsc.* **131** (1982) 259–263.
9. J. McELANEY, N. ALEM and V. ROBERTS, ASME Pub. No. 70-WA/BHF-2, 1–9.
10. R. T. DeHOFF, E. H. AIGELTINGER and K. R. CRAIG, *J. Microsc.* **95** (1972) 69–91.
11. R. W. E. MELLISH, W. FERGUSON-PELL, G. V. B. COCHRAN, R. LINDSAY and D. W. DEMPSTER, *J. Bone and Mineral Res.* **6** (1991) 689–697.
12. A. VESTERBY, H. J. G. GUNDERSEN and F. MELSEN, *Bone* **10** (1989) 7–13.
13. I. SINGH, *J. Anatomy* **127** (1978) 305–310.
14. L. A. FELDKAMP, S. A. BOLDSTEIN, A. M. PARFITT, G. JESION and M. KLEEREKOPER, *J. Bone and Mineral Res.* **4** (1989) 3–11.
15. N. J. GARRAHAN, R. W. E. MELLISH and J. E. COMPSTON, *J. Microsc.* **142** (1986) 341–349.
16. J. A. QUIBLIER, *J. Colloid and Interface Sci.* **98** (1983) 84–102.
17. E. LOZUPONE and A. FAVIA, *Calcified Tiss. Int.* **46** (1990) 367–372.
18. D. P. FYHRIE, N. L. FAZZALARI, R. GOULET and S. A. GOLSTEIN, *J. Biomechanics* **26** (1993) 955–967.
19. R. W. GOULET, L. A. FELDKAMP, D. J. KUBINSKI and S. A. GOLDSTEIN, In Proceedings of 35th Annual Meeting, Orthopaedic Research Society, February 6–9 (1989).
20. J. E. AARON, D. R. JOHNSON, J. A. KANIS, B. A. OAKLEY, P. O'HIGGINS and S. K. PAXTON, *Computer and Biomed. Res.* **25** (1992) 1–16.
21. E. POLIG and W. E. E. JEE, *Bone* **6** (1985) 357–359.
22. N. J. GARRAHAN, R. W. E. MELLISH, S. VEDI and J. E. COMPSTON, *ibid.* **8** (1987) 227–230.
23. A. D. KUO and D. R. CARTER, *J. Orthop. Res.* **9** (1991) 918–931.
24. P. RAUX, P. R. TOWNSEND and R. MIEGEL, *J. Biomechanics* **8** (1975) 1–7.
25. M. YANUKA, F. A. L. DULLIEN and D. E. ELRICK, *J. Microsc.* **135** (1984) 159–168.
26. M. J. KWIECIEN, I. F. MAC DONALD and F. A. L. DULLIEN, *ibid.* **159** (1990) 343–359.
27. I. F. MAC DONALD, P. KAUFMANN and F. A. L. DULLIEN, *ibid.* **144** (1986) 277–296.
28. H. TAGAI and H. AOKI, *Mechanical Properties of Biomaterials*, edited by G. W. Hastings and D. F. Williams (John Wiley & Sons, 1980) pp. 477–488.
29. I. M. O. KANGASNIEMI, K. de GROOT, J. G. M. BECHT and A. YLI-URPO, *J. Biomed. Mater. Res.* **26** (1992) 663–674.
30. A. H. BURSTEIN, J. M. ZIKA, K. G. HEIPLE and L. KLEIN, *J. Bone & J. Surg.* **57A** (1975) 956–961.
31. C. H. TURNER, *J. Biomechanical Engng* **111** (1989) 256–259.
32. F. LINDE, I. HVID and F. MADSEN, *J. Biomechanics* **26** (1992) 359–368.
33. T. M. KEAVENY, R. E. BORCHERS, L. J. GIBSON and W. C. HAYES, *ibid.* **26** (1993) 991–1000.

Received 4 May
and accepted 5 May 1995